Dual-demodulation large-scope high-sensitivity refractive index sensor based on twin-core PCF*

LI Chen-yuan (李宸源)[1], **SONG Bin-bin** (宋彬彬)[1]**, **WU Ji-xuan** (吴继旋)[2], **HUANG Wei** (黄薇)[1], **WU Xu-jie** (吴徐洁)[1], **and JIN Chang** (靳畅)[1]

1. *The Key Laboratory of Computer Vision and System of Ministry of Education, Tianjin Key Laboratory of Intelligence Computing and Novel Software Technology, Tianjin University of Technology, Tianjin 300384, China*
2. *Tianjin Key Laboratory of Optoelectronic Detection Technology and Systems, College of Electronic and Information Engineering, Tiangong University, Tianjin 300387, China*

(Received 29 February 2020; Revised 23 September 2020)

In this paper, a refractive index (RI) sensor based on the twin-core photonic crystal fiber (TC-PCF) is presented. Introducing the rectangular array in the core area makes the PCF possible to obtain high birefringence and low confinement loss over the wavelength range from 0.6 μm to 1.7 μm. Therefore, the core region can enhance the interaction between the core mode and the filling material. We studied theoretically the evolution characteristics of the birefringence and operating wavelength corresponding to the strongest polarization point under the condition of filling the rectangular array with RI matching fluid range from 1.33 to 1.41. Simulation results reveal that the proposed TC-PCF has opposite evolutions of change rates between the *B* and wavelength, and the maximum RI sensing sensitivities of 1.809×10^{-2} B/RIU and 8 700 nm/RIU at low and high RI infill are obtained respectively, which means that the TC-PCF features of dual-parameter demodulation for the RI sensing can maintain a high refractive index sensing sensitivity within a large scope of RI ranging from 1.33 to 1.41. Compared with the results of single-parameter demodulation, it is an optimized method to improve the sensitivity of low refractive index sensors, which has great application potency in the field of biochemical sensing and detection.

Document code: A **Article ID:** 1673-1905(2021)04-0193-6

DOI https://doi.org/10.1007/s11801-021-0129-z

In recent years, photonic crystal fiber (PCF) has received a tremendous research attention and has been used for optical functional devices widely[1]. Due to the remarkable light guiding properties, abundant model features and flexible structural characteristics[2-8], the PCFs provide new ideas for scientific researchers to broaden the field of sensors. All kinds of PCF-based sensors were investigated such as temperature sensors[9], gas sensors[10], stress sensors[11], chemical sensors[12,13], pH sensors[14], biosensors[15,16], refractive index (RI) sensors[17] and so on. Concurrently they are developing in the direction of small and flexible, high sensitivity, good stability, strong environmental adaptability, and accurate measurement results. The RI sensors based on PCFs of which are more prominent attributing to the selective filling of air holes, the mode characters and propagating behavior would be changed and tuned by filling partial air holes as required. In addition, the air holes limit the interaction between the mode field and the inner filled liquid in a micron scaled area, which is very advantageous for trace sample detection. Therefore, the PCF-based RI sensors play an important role in the field of biological detection, medical diagnosis, environmental safety, etc., especially for the global public health events such as the detection of COVID-19.

The existing RI sensing technologies include two methods, the external sensing and internal sensing. The external sensing methods generally utilize optical fiber reprocessing technologies (such as side polishing[18], fabricating fiber grating[19], etc.) to construct the interact region of liquid and light field, and most of them are based on evanescent field sensing. However, the evanescent field indirectly affects the light transmission characteristics of guided mode, which limits the sensitivity of this RI sensor to not be high. While the internal sensing is a method based on the technology of selective filling air holes, the inner filled liquid directly affects the mode characters in the same area of PCFs, which results in an intense

* This work has been supported by the National Natural Science Foundation of China (Nos.11804250, 11904262 and 11704283), the Tianjin Natural Science Foundation (No.18JCQNJC71300), the Tianjin Education Commission Scientific Research Project (No.2018KJ146), and the Opening Foundation of Tianjin Key Laboratory of Optoelectronic Detection Technology and Systems (No.2019LODTS004).
** E-mail: bbsong@email.tjut.edu.cn

light matter interaction and high RI sensing sensitivity. Most of the current studies use one parameter to demodulate the RI sensing sensitivity, and the RI sensing sensitivity changes almost monotonously, it is difficult to maintain high sensing sensitivity over a wide range of RI, which limits the range of applications of RI sensors. How to improve the sensing sensitivity in the low or high RI range that was insensitive for the RI sensors of single parameter demodulation? It is an urgent problem to be solved in order to increase the RI sensing scope of RI sensors.

The birefringent PCFs integrate with the technology of selective filling could tune the birefringent values, which is one of the excellent candidate methods of RI sensing. Thus, multiple RI sensors based on asymmetric structures of PCFs with high birefringence have been reported such as hexagonal structure with elliptical and circular air holes[20], designs with all circular air holes[21], and distributions with different sizes of circular air holes[22]. Although the study has simultaneously achieved high birefringence of 10^{-3} order, it is difficult and expensive to fabricate the PCFs consisted of circular and elliptical air holes. The PCFs arrayed with all circular air holes are manufactured conveniently by contrast, and their polarization performances could be tuned flexibly utilizing the method of selective filling which could also observe the more optimized effect as that of elliptical air holes.

In this paper, a highly birefringence PCF based on rectangular array introduced in the twin core area was designed, where the air holes in the core and cladding are all circular. The proposed TC-PCF can realize high RI sensing sensitivity within a large RI range by simultaneously demodulating the variation of birefringence and wavelength. Through numerically investigating, we found that the maximum birefringence of $1.448\,4\times10^{-3}$ was obtained at the wavelength of 1.297 μm and RI of 1.33, the RI sensing sensitivities for birefringence demodulation decrease monotonously as the inner filled RI increase, and the maximum reaches up to 1.809×10^{-2} B/RIU at the low RI of 1.33; the RI sensing sensitivities for wavelength demodulation show an inverse trend to that of birefringence demodulation, and the maximum reaches up to 8 700 nm/RIU at the high RI of 1.41. This means that TC-PCF greatly enlarged the RI detection scope range from 1.33 to 1.41 thoroughly with high sensing sensitivity. Due to the proposed TC-PCF sensor has the advantages of large sensing scope, small volume, high sensitivity, high birefringence and easy manufacture, it can be widely used in environment quality-detection and medical diagnosis.

In this work, a refractive index-guided birefringence PCF was proposed and analyzed, its structure of cross section is shown in Fig.1. The background material is pure silica, and distributing a hexagon array consisted of four layers air holes in the cladding area, of which the diameter of air holes in the innermost ring and the outer three rings are d_1=1.5 μm and d=1.9 μm, respectively, and the pitch between the two air holes in the cladding is set to Λ=2.4 μm. As presented in Fig.1, one of the special features of the proposed PCF is that the central region was designed with a rectangular arrangement formed by two rows circle-air holes. The cross-sectional view of the TC-PCF core region is enlarged shown in the inset, where the pitch of holes is Λ_c=0.6 μm and the uniform diameter of air holes is d_c=0.56 μm respectively. According to the structure of TC-PCF, the polarization characteristics would become apparent due to the asymmetrical rectangular array is introduced in the core area, and the twin core is formed in the central silica area which is separated into two portions in the direction of x, of which the mode fields are deeply restrained in the y direction and probably divided into the two cores in the x direction. When the rectangular array is filled with the targeted liquid, the restrain ability to mode field would be tuned, which results in the polarization characteristics of TC-PCF changing correspondingly.

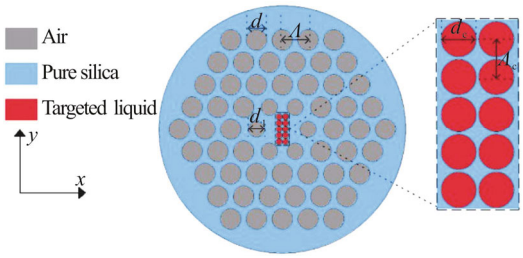

Fig.1 Transverse cross section of the proposed TC-PCF showing the microstructure core diameter d_c, pitch Λ_c in the core, diameter of holes in the innermost ring d_1, diameter of holes in the three outermost claddings d, and pitch in the cladding Λ

The finite element method (FEM) is applied for solving many complex geometric domain and can provide full vector analysis of different photonic waveguide devices[23-26] due to its confirmed reliability. So it is perfect that utilizing the FEM to analyze the properties of optical field in PCF, the commercial software COMSOL Multiphysics 5.2 is adopted for the analysis of the structure. To compute the leakage loss, an effective boundary condition is needed, which produces no reflection at the boundary. Perfectly matched layers (PMLs) are anisotropic perfectly matched layers with high absorption properties. By using PMLs as a boundary condition, propagation characteristics and optical properties of leaky modes in PCFs can be precisely calculated. This method is independent of the fiber structure parameters, and can be applied to any size, shape and structure of the cladding air holes in photonic crystal fibers. The modal analyses have been performed on the cross section in the x-y plane of the PCF structure as the wave is propagating in the z direction. We assumed the circular PML[27], where magnetic field satisfies the Maxwell's equations:

$$\nabla\times(\varepsilon_\gamma^{-1}\nabla\times H)-k_0^2\mu_\gamma H=0, \quad (1)$$

where ε_γ and μ_γ are the relative dielectric permittivity and magnetic permeability respectively. The symbol $k_0=2\pi/\lambda$ is the wave number in a vacuum, where λ is the operating wavelength. H is the magnetic field vector, which can be expressed as $H=h(x,y)\exp(-j\beta z)$, where $h(x,y)$ is the field distribution on the transverse plane, the propagation constant β is represented by the following equation:

$$\beta=n_{\text{eff}}k_0. \quad (2)$$

Based on the complex modal effective index n_{eff}, the propagation constant β and the modal birefringence can be obtained.

The modal birefringence (B) is an important parameter to define the polarization property of birefringent fibers, which represents the effective refractive indexes difference between the two polarized modes of fundamental mode along x and y direction, therefore, the B could be expressed as follows:

$$B=|\text{Re}(n^x_{\text{eff}}-n^y_{\text{eff}})|, \quad (3)$$

where n^x_{eff} and n^y_{eff} are the effective refractive indexes of the X and Y polarized fundamental mode respectively, and Re represents the real part of the effective refractive index.

One characteristic parameter related to birefringence is beat length, which could be measured directly by the method of different group delay. The polarization beat length L_B between two orthogonal polarization modes is[28]:

$$L_B=\frac{\lambda}{B}. \quad (4)$$

Due to a finite number of air holes in the cladding part, the leakage of light from core to exterior matrix material occurs through bridges between air holes, which results in confinement losses. The confinement loss strongly depends on the number of layers, number of air holes, air hole diameter and the pitch of holes spacing. The confinement loss (dB/m) is determined from the imaginary part of the complex effective index, which could be expressed as[29]:

$$CL=\frac{40\pi}{\ln(10)\lambda}I_m(n_{\text{eff}}), \quad (5)$$

where $I_m(n_{\text{eff}})$ is the imaginary part of the effective refractive index of the core modes.

The TC-PCF performed the strongest polarization characteristic at a certain wavelength consequentially within the operating wavelength range from 0.6 μm to 1.7 μm, which is the maximum birefringence could be observed under the point with the strongest polarization characteristic, which for convenient terming characteristic point for short in the following. The RI sensing sensitivities are evaluated by using the two parameters of birefringence and wavelength corresponding to the same characteristic point. There probably be differences between the evolution laws of B and wavelength with the changes of infilled refractive index, and the differences could be significantly magnified by taking the derivative of these changes, which also represents the RI sensing sensitivities, the derivative expressions are defined as

$$\begin{cases} S_\lambda=\partial\lambda_{\text{peak}}/\partial n_a \\ S_B=\partial B_{\text{peak}}/\partial n_a \end{cases}, \quad (6)$$

where λ_{peak} and B_{peak} represent the wavelength and birefringence of characteristic point and n_a is the RI of analyte infilled in the rectangular array area. By taking the derivative of the variations of wavelength and birefringence respectively, dual parameters demodulation for the RI sensing sensitivity would be achieved with different units of nm/RIU and B/RIU severally.

The mode fields distribution of TC-PCF are investigated to interpret the polarization dependent characteristic. Fig.2 shows the resultant 2D views of mode field profiles of X and Y polarized fundamental modes under different RI ranging from 1.33 to 1.41. As shown in the mode field profiles, due to the introduction of rectangular array of air holes in the core area, the central area of the silica is divided into two parts in the x direction, and the fundamental modes almost distribute in the two separated silica

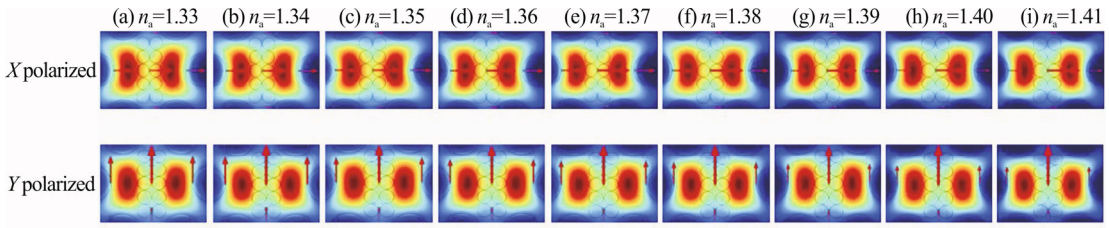

Fig.2 Electric field distributions of the *X* and *Y* polarized fundamental modes under different RI infilled in rectangular array core area ranging from 1.33 to 1.41

areas. It is obvious that the fundamental mode fields are immensely confined in the y direction and extended in the x direction, this is accounted for there are more boundary restrictions in the y direction than in the x direction attributed to the configuration of core and cladding air holes. When the rectangular array of air holes are infilled with target liquid, the boundary condition of rectangular array was tuned regularly, which results in the polarization dependent characteristic changing between the X and Y polarized fundamental modes, which

is consistent with the above theoretical analysis.

Fig.3 presents the effective RI curves as a representative of *X* and *Y* polarized fundamental modes of the proposed TC-PCF under the infilled RI of 1.33, 1.34 and 1.35 severally. The effective RI curve of silica is offered as contrast referenced the Sellmeier formulas[30]. It is obvious that the effective RI of fundamental modes are much less than the RI of silica due to the high air filling ratio in the PCF core area, and they decrease with the wavelength increases. As the infilled RI increasing, the equivalent RI of material increase in the solution domain, which results in the increasing of the effective RI of fundamental modes. The effective RI curves also demonstrate the polarization feature of TC-PCF is that the effective RI of *Y* polarized modes are all larger than the *X* polarized modes, which because of the electric field lines of *Y* polarized modes are parallel to the long side of the rectangular array, the mode field of the *Y* polarized mode is mainly confined in the two silica areas on both sides of the rectangular array in the *x* direction, however, the electric field lines of *X* polarized modes are perpendicular to the long side of the rectangular array, resulting its mode field energy is distributed in the two separate silica areas but also in the rectangular array of air holes. Therefore, the effective mode field area of the *X* polarized mode is larger than the *Y* polarized mode, which arouses consequently the effective RI of the *X* polarized mode is smaller than that of the *Y* polarized mode.

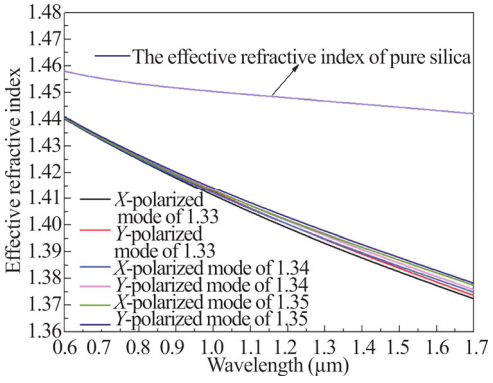

Fig.3 Effective refractive indices of the fundamental modes for *X* and *Y* polarization under different RI ranging from 1.33 to 1.35

The measurement of mode confinement of the guided light is also one of the key parameters in the practical applications. Variation of the confinement loss as a function of refractive index liquids are illustrated in Fig.4. It can be seen that the confinement loss increases with the wavelength increases, but keeping the extremely low index of $3.945\ 57\times10^{-11}$ dB/m below the wavelength of 1 400 nm. In addition, the lower confinement losses are achieved when the RI of the infilled liquid increases. The minimum confinement loss of the PCF is $8.905\ 62\times10^{-13}$ dB/m, when λ=1.09 μm with RI of 1.41.

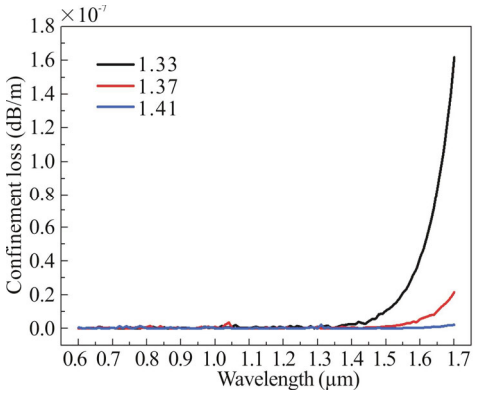

Fig.4 The curve of confinement loss vs. wavelength for varying RI liquids with 1.33, 1.37 and 1.41, respectively

According to Eq.(3), *B* could be observed by taking from the difference of effective RI of *X* and *Y* polarized modes. The relationships between *B* and wavelength under different infilled RI ranging from 1.33 to 1.41 are shown in Fig.5(a). It can be seen that the birefringence curves of the fundamental mode increase at first and then decrease with the wavelength increasing. At a certain wavelength between 0.6 μm to 1.7 μm, *B* reaches a maximum value. The point where *B* reaches the maximum value performs the strongest point of the polarization characteristic, that is "characteristic point", which is consistent with the theoretical analyzing in the above. The characteristic points have a blue shift and its *B* tend to decreasing with different RI filling conditions. Fig.5(b) was plotted by using the characteristic point of each birefringence curve in Fig.5(a), it describes the evolution tendencies of *B* (black line) and wavelength (blue line) dependent on different RI ranging from 1.33 to 1.41, of which the maximum *B* is achieved at the wavelength of 1.297 μm and RI of 1.33, and then it performs decreasing from the maximum of $1.448\ 4\times10^{-3}$ to 2.984×10^{-4}. It can be seen that lower RI is reaching the higher *B*. It is also clear that the wavelength of characteristic point has a blue shift from 1 297 nm to 736 nm with an increased infilled RI. Moreover, although the trend curves of *B* and wavelength of the characteristic points are both decreasing, there is a slight difference in the rate of change, which can be amplified by taking from the derivative of the evolution tendencies.

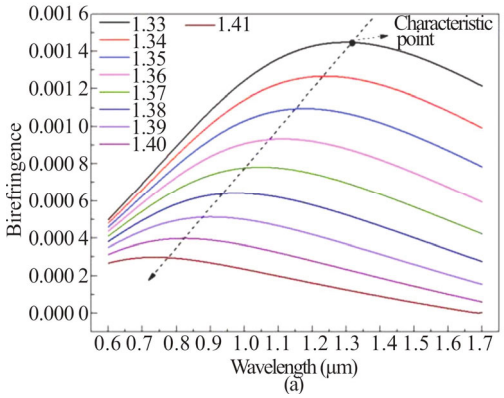

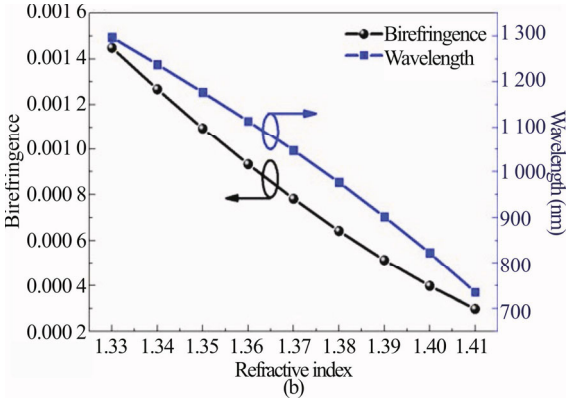

Fig.5 (a) Birefringence versus wavelength of the infilled TC-PCF; (b) Variation curves of birefringence and wavelength of the characteristic point with the RI ranging from 1.33 to 1.41

The RI sensing sensitivities are obtained by taking from derivation of the variation of B and wavelength according to Eq.(6), which are displayed in Fig.6. It shows more clearly the difference between the change rate of B and wavelength. The RI sensing sensitivities are demodulated dually by the two parameters of B and wavelength, of which the B-demodulated RI sensing sensitivity is expressed by the black dotted line, the wavelength-demodulated results are displayed by the blue dotted line. It's observed that the RI sensing sensitivities demodulated by B decrease with the RI increasing while the wavelength-demodulated RI sensing sensitivities perform the opposite tendency, the maximum RI sensing sensitivities demodulated by B and wavelength are achieved up to 1.809×10^{-2} B/RIU and 8 700 nm/RIU at the lowest RI of 1.33 and the highest RI of 1.41, respectively, in order to facilitate the analysis, the negative sign of RI sensing sensitivities are not be considered. The reason behind the opposite evolutions is that with the RI of the infilled liquid increasing, the restricted ability of the rectangular array to the optical field becomes weakening, and the difference of equivalent RI of material between the x-direction and y-direction in the central area of the TC-PCF diminishing, which results in the polarization characteristics of TC-PCF weakening and the B becomes smaller accordingly. In addition, the influence of increased infilled RI on the effective RI of a certain mode is greater than that of the effective RI difference of the modes, so the wavelength change of the characteristic point is more obvious, which results in the RI sensing sensitivity demodulated by wavelength gradually increasing, and the B-demodulated RI sensing sensitivity gradually decreasing, as the RI sensing sensitivities are comparatively shown in Tab.1. The dual parametric demodulation method features two completely opposite RI sensing performances, which means that a suitable RI sensor demodulation method could be observed to maintain the sensor keeping the optimal RI sensing performance in the wide RI range from 1.33 to 1.41. For example, the B-demodulated method is optimum in the RI lower 1.38, the wavelength-demodulated method is more appropriate in the RI higher 1.38, which greatly enlarges the RI sensing scope and broadens its application fields. Therefore, due to the advantages of dual demodulation, large RI sensing scope, high RI sensing sensitivity and so on. The TC-PCF has the great potential for application in the fields of low RI biochemical and high RI heavy metal detection.

Tab.1 The dual-demodulation RI sensing sensitivities of the sensor with infilled RI ranging from 1.33 to 1.41

RI	S_λ (nm/RIU)	S_B (B/RIU)
1.33	5 900	0.018 09
1.34	6 000	0.017 63
1.35	6 200	0.016 69
1.36	6 500	0.015 68
1.37	6 850	0.014 59
1.38	7 250	0.013 42
1.39	7 700	0.012 15
1.40	8 300	0.010 77
1.41	8 700	0.010 05

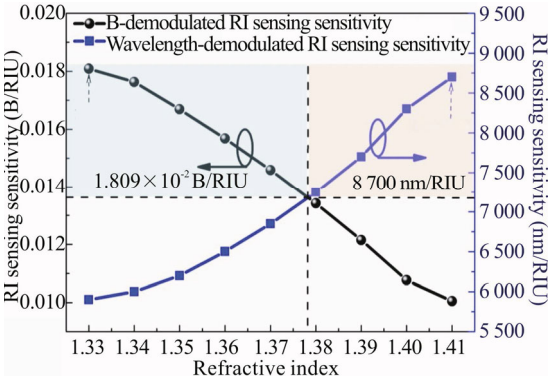

Fig.6 The changes of dual-demodulation RI sensing sensitivities

Fig.7(a) indicates the beat length as a function of the wavelength. It can be seen that the beat length increases with the wavelength and RI increase, the beat length corresponding to the characteristic points were marked and shown in Fig.7(b), it describes the evolution of different RI range of L_B from 1.33 to 1.41, and the RI sensing sensitivities of L_B is obtained by taking from the derivation, we convert the B-demodulated RI sensing sensitivities to that of L_B-demodulated, which is more convenient to detect in practice.

In conclusion, a highly sensitive, dual demodulated and large sensing scope RI sensor based on TC-PCF has been designed and investigated. Due to the air holes in the core and cladding are all circular, the manufacturing complexity is reduced. The rectangular array of air holes in the PCF core area introduced a high birefringence character, and the infilled RI liquid in the rectangular array tuned the polarization performance. The maximum RI sensing sensitivities of 1.809×10^{-2} B/RIU and 8 700 nm/RIU at low and high RI infilled were obtained

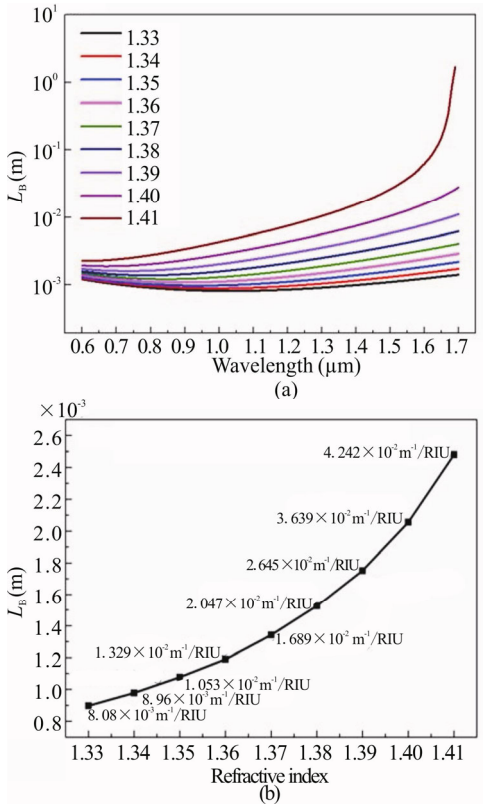

Fig.7 (a) Beat length as a function of the wavelength for different RI; (b) The curve of beat length with RI corresponding to characteristic points

respectively employing dual demodulation method. The *B* and wavelength of the maximum polarization point had totally different and opposite change rates, which ensured the proposed sensor always performing the optimal RI sensing sensitivities over a wide RI sensing scope. Therefore, the proposed TC-PCF reveals great potential impact on future applications in the low RI biochemical and high RI heavy metal detection.

References

[1] R. F. Cregan, B. J. Mangan, J. C. Knight, T. A. Birks, P. S. Russell, P. J. Roberts and D. C. Allan, Science **285**, 1537 (1999).

[2] J. C. Knight, T. A. Birks, P. S. Russell and D. M. Atkin, Optics Letters **21**, 1547 (1996).

[3] J. C. Knight and P. S. J. Russell, Science **296**, 276 (2002).

[4] K. Tajima, J. Zhou, K. Nakajima and K. Sato, Journal of Lightwave Technology **22**, 7 (2004).

[5] H. Ademgil, Optik **125**, 6274 (2014).

[6] A.M. Pinto and M. Lopez-Amo, Journal of Sensors **2012**, 1 (2012).

[7] T. A. Birks, J. C. Knight and P. St. J. Russell, Optics Letters **22**, 961 (1997).

[8] Y. Liu and H. W. M. Salemink, Europhysics Letters **107**, 1160 (2014).

[9] Y. H. Chang, Y. Y. Jhu and C. J. Wu, Optics Communications **285**, 1501 (2012).

[10] Y. N. Zhang, Y. Zhao and Q. Wang, Sensors & Actuators: B. Chemical **184**, 179 (2013).

[11] T. W. Lu and P. T. Lee, Optics Express **17**, 1518 (2009).

[12] W. C. Lai, S. Chakravarty, Y. Zou and R. T. Chen, Optics Letters **38**, 3799 (2013).

[13] S. Zheng, Y. Zhu and S. Krishnaswamy, Nano-film-Coated Photonic Crystal Fiber Long-Period Gratings with Modal Transition for High Chemical Sensitivity and Selectivity, Proceedings of SPIE - The International Society for Optical Engineering **8346**, 1844 (2012).

[14] P. Hu, X. Dong, W. C. Wong, L. H. Chen, K. Ni and C. C. Chan, Applied Optics **54**, 2647 (2015).

[15] E. K. Akowuah, T. Gorman, H. Ademgil, S. Haxha, G. K. Robinson and J. V. Oliver, IEEE Journal of Quantum Electronics **8**, 1403 (2012).

[16] T.M. Monro, W. Belardi, K. Furusawa, J.C. Baggett, N.G.R. Broderick and D.J. Richardson, Measurement Science and Technology **12**, 854 (2001).

[17] X. L. Lu, X. D. Zhang, N. Chen, M. Chang and B. X. Li, Optik **220**, 165021 (2020).

[18] K. K. Guo, H. Jun, S. Q. Cao, M. X. Hou, Z. Zhe, G. X. Xu and Y. P. Wang, Optics Express **26**, 34699 (2018).

[19] B. C. Wang, L. Y. Ren, X. D. Kong, Y. P. Xu, K. L. Ren, W. X. Yang, S. B. Cheng, F. Chen and F. Song, Optik **207**, 164454 (2020).

[20] M. F. H. Arif and M. J. H. Biddut, Sensing and Bio-Sensing Research **12**, 8 (2017).

[21] M. F. H. Arif and M. J. H. Biddut, Optik **131**, 697 (2017).

[22] H. Ademgil and S. Haxha, Optik **127**, 6653 (2016).

[23] Y. L. Hoo, W. Jin, H. L. Ho, D. N. Wang and R. S. Windeler, Optical Engineering **41**, 8 (2002).

[24] J. B. Jensen, P. E. Hoiby, G. Emiliyanov, O. Bang, L. H. Pedersen and A. Bjarklev, Optics Express **13**, 5883 (2005).

[25] B. T. Kuhlmey, B. J. Eggleton and D. K. C. Wu, Journal of Lightwave Technology **27**, 1617 (2009).

[26] M. Vieweg, T. Gissibl, S. Pricking, B. T. Kuhlmey, D. C. Wu, B. J. Eggleton and H. Giessen, Optics Express **18**, 25232 (2010).

[27] J. Park, S. Lee, S. Kim and K. Oh, Optics Express **19**, 1921 (2011).

[28] M. Liu, H. T. Yuan, P. Shum, C. Shao, H. N. Han and L. H. Chu, Applied Optics **57**, 6383 (2018).

[29] H. L. Chen, S. G. Li, G. W. An, J. S. Li, Z. K. Fan and Y. Han, Plasmonics **10**, 57 (2015).

[30] I. H. Malitson, Journal of the Optical Society of America **55**, 1205 (1965).